Cavβ3 Regulates Ca^{2+} Signaling and Insulin Expression in Pancreatic β-Cells in a Cell-Autonomous Manner

Alexander Becker, Barbara Wardas, Houssein Salah, Maryam Amini, Claudia Fecher-Trost, Qiao Sen, Damian Martus, Andreas Beck, Stephan E. Philipp, Veit Flockerzi, and Anouar Belkacemi

Diabetes 2021;70:2532–2544 | https://doi.org/10.2337/db21-0078

Voltage-gated Ca^{2+} (Cav) channels consist of a pore-forming Cavα1 subunit and auxiliary Cavα2-δ and Cavβ subunits. In fibroblasts, Cavβ3, independent of its role as a Cav subunit, reduces the sensitivity to low concentrations of inositol-1,4,5-trisphosphate (IP_3). Similarly, Cavβ3 could affect cytosolic calcium concentration ($[Ca^{2+}]$) in pancreatic β-cells. In this study, we deleted the Cavβ3-encoding gene *Cacnb3* in insulin-secreting rat β-(Ins-1) cells using CRISPR/Cas9. These cells were used as controls to investigate the role of Cavβ3 on Ca^{2+} signaling, glucose-induced insulin secretion (GIIS), Cav channel activity, and gene expression in wild-type cells in which Cavβ3 and the IP_3 receptor were coimmunoprecipitated. Transcript and protein profiling revealed significantly increased levels of insulin transcription factor Mafa, CaMKIV, proprotein convertase subtilisin/kexin type-1, and nitric oxide synthase-1 in Cavβ3-knockout cells. In the absence of Cavβ3, Cav currents were not altered. In contrast, CREB activity, the amount of MAFA protein and GIIS, the extent of IP_3-dependent Ca^{2+} release and the frequency of Ca^{2+} oscillations were increased. These processes were decreased by the Cavβ3 protein in a concentration-dependent manner. Our study shows that Cavβ3 interacts with the IP_3 receptor in isolated β-cells, controls IP_3-dependent Ca^{2+}-signaling independently of Cav channel functions, and thereby regulates insulin expression and its glucose-dependent release in a cell-autonomous manner.

The increase in blood glucose concentration triggers Ca^{2+} oscillations in pancreatic β-cells and leads to insulin secretion (1–4). These Ca^{2+} oscillations are composed of Ca^{2+} influx, which occurs predominantly via voltage-gated Ca^{2+} (Cav) channels, and Ca^{2+} release from intracellular stores via intracellular ion channels, the inositol-1,4,5-trisphosphate receptors (IP_3R) (5,6), and the ryanodine receptors (7).

Cav channels consist of a pore-forming α1 subunit and auxiliary subunits β, α2-δ, and, in skeletal muscle, γ (8). The β subunits form a family of cytosolic proteins encoded by four genes, *Cacnb1–4*, which influence the plasma membrane targeting of the α1 subunit and affect the channel function. For example, Cavβ3 increases the surface expression of Cav1.2 in vascular smooth muscle cells (9) and Cavβ2 in pancreatic β-cells (10). In contrast, in cardiomyocytes, β-adrenergic stimulation of Cav currents (11) but not the plasma membrane targeting of the Cav1.2 ion-conducting pore depends on the presence of Cavβ2 (11,12).

In pancreatic β-cells, deletion of the genes of the Cav1.2 (13) and Cav2.3 (14,15) or of the α2-δ1 subunit (16) leads to a reduction in Cav currents and thus to decreased insulin release and worsened glucose tolerance. In contrast, removal of the Cavβ3 leads to more efficient glucose clearance without compromising the Cav channel function (17,18). In fibroblasts isolated from mouse tissue, Cavβ3 decreases their sensitivity to low concentrations of IP_3 (19), thereby modulating Ca^{2+} release from intracellular stores with effects on cell migration in vitro and skin wound healing in vivo (19,20). This function of Cavβ3 occurs independently of its role as a Cav channel subunit and requires Cavβ3 to interact with the IP_3R.

For the above studies (17–19), Cavβ3-knockout (KO) mouse lines in which the *Cacnb3* gene was deleted throughout the organism were used as controls. To

Institut für Experimentelle und Klinische Pharmakologie und Toxikologie, Präklinisches Zentrum für Molekulare Signalverarbeitung der Universität des Saarlandes, Homburg, Germany

Corresponding author: Anouar Belkacemi, anouar.belkacemi@uks.eu

Received 31 January 2021 and accepted 12 August 2021

This article contains supplementary material online at https://doi.org/10.2337/figshare.15173556.

A.Bec. and B.W. contributed equally to this work.

investigate the extent to which Cavβ3 determines the observed phenotype in the absence of other cell types in pancreatic β-cells alone, independent of cell networks, we used insulin-secreting insulinoma (Ins-1) rat β-cells in this study. We examined the interaction of Cavβ3 with the IP_3R and its influence on insulin biogenesis and secretion. As controls, we used Cavβ3-deficient cells generated by CRISPR/Cas9.

RESEARCH DESIGN AND METHODS

Generation of Cavβ3-Deficient Rat Insulinoma Ins-1 Cell Line

A Cavβ3-deficient cell clone was generated using CRISPR/Cas9 as described (21). Briefly, the target sequence within exon4 of the *Cacnb3* gene, 5′-GC CGG ATG CTC TCC AGG CGT TGG-3′ (Fig. 1*A*), was identified using CRISPR.MIT.EDU (22) and E-CRISP (23), and possible off-target sequences were excluded using Cas-OFFinder (24). The target sequence was inserted into pGS-U6-gRNA (GenScript) and cotransfected with pcDNA3.3-Cas9–2A-eGFP into Ins-1 cells. Single green-fluorescent cells were isolated and expanded. Genomic *Cacnb3* fragments of single clones were amplified by PCR using oligonucleotide primers 5′-T ACA GCA ATG ACT GGT GGA TCG-3′ (exon4) and 5′-T TAT GAC AGC TGG GCA TCT ACG-3′ (intron 4–5) and examined for mutations by lack of *Bsl*I restriction cut and sequencing of both strands.

Cell Culture and Transfection

Ins-1 were cultured at 37°C and 5% CO_2 in RPMI 1640 medium containing 11.1 mmol/L D-glucose and supplemented with 10% FCS, 1 mmol/L sodium pyruvate, 1 mmol/L HEPES, 50 μmol/L 2-mercaptoethanol, 10,000 units/mL penicillin, and 10 mg/mL streptomycin. Cells were transfected with Cavβ3 cDNA-encoding plasmids (19) using Lipofectamine 3000 (Thermo Fisher Scientific).

RNA Isolation and Transcriptome Sequencing

RNA was isolated from Ins-1 cells using the RNeasy Mini PLUS Kit (#74134; Qiagen). The RNA quality was evaluated, and only samples (1 μg total RNA) with RNA quality indicator values >9.3 were used to generate sequencing

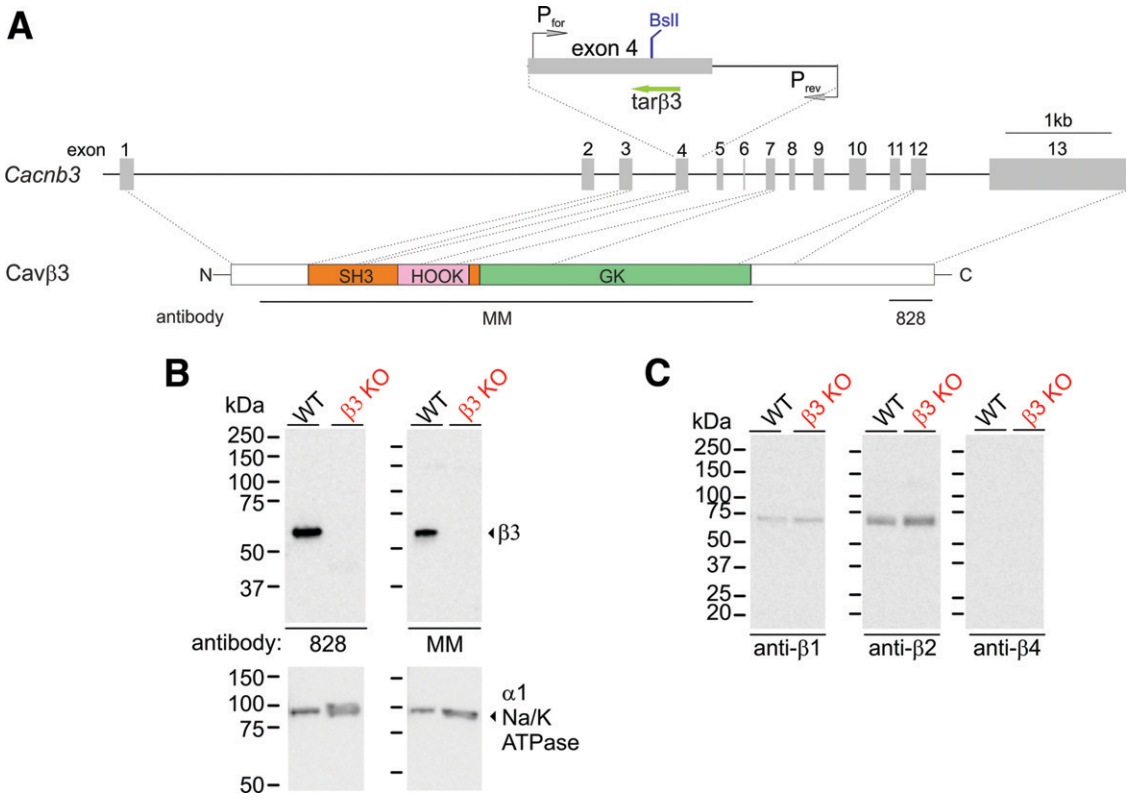

Figure 1—Generation of Cavβ3-deficient β-cells. *A*: CRISPR/Cas9-based strategy to delete the *Cacnb3* gene. The positions of the target sequence for the guide RNA tarβ3, of the restriction enzyme *Bsl*I site present in wild-type and absent in the introduced mutation, and of the oligonucleotide primers used to amplify Cavβ3 fragments are indicated (top). The *Cacnb3* gene (middle), the Cavβ3 protein domains (bottom) (N, N-terminus [white]; SH3, Src-homology 3 [orange]; HOOK [pink]; GK, guanylate kinase [green]; C, C-terminus [white]), and the Cavβ3 fragments used to generate the anti-Cavβ3 antibodies MM and 828 are indicated. Western blot of protein extracts from wild-type (WT) and Cavβ3-KO Ins-1 β-cells (100 μg protein/lane) using antibodies against the Cavβ3 (*B*) and Cavβ1, β2, and β4 (*C*). Western blots indicate the absence of Cavβ3 protein in Cavβ3-KO cells and the presence of Cavβ1, β2, and β3 but not of Cavβ4 in WT cells. The α-subunit of the Na^+/K^+ ATPase protein served as a loading control (*B*).

libraries, which were generated using NEBNext Ultra RNA Library Prep Kit for Illumina (New England Biolabs). Clustering of the index-coded samples was performed on a cBot Cluster Generation System using the PE Cluster Kit cBot-HS (Illumina). The library preparations were sequenced, and paired-end reads were generated. Gene model annotation files and reference genome were downloaded from the National Center for Biotechnology Information/University of California, Santa Cruz/Ensembl. The HISAT2 software was used to map paired-end clean reads, and the fragments per kilobase of transcript per million mapped reads (FPKM) of each gene were calculated based on the length of the gene and reads count mapped to this gene.

Nano-Liquid Chromatography–High-Resolution Mass Spectrometry and Raw Data Analysis

Independent protein lysates from wild-type and Cavβ3-KO β-cells were denatured, separated on SDS-PAGE, prepared for mass spectrometry, and analyzed by nano-liquid chromatography–high-resolution mass spectrometry as described (25). Tryptic peptides were identified using the Mascot algorithm and Proteome Discoverer software 1.4 (Thermo Fisher Scientific). Peptides and derived fragments were analyzed with Mascot 2.4.0 by searching a Swiss-Prot database. Peptide and fragment spectra were matched allowing a mass tolerance of 7 parts per million for precursor masses and 0.5 Da for peptide fragment ions. We used tryptic digestion and allowed for up to two missed cleavage sites. Cysteine carbamidomethylation was set as a fixed modification and deamidation of asparagine, and glutamine, acetylation of lysine, and oxidation of methionine were set as variable modifications. The Mascot output files were loaded in the software Scaffold and to ensure significant protein identification, the protein probability filter was set to 99%, resulting in a false discovery rate (FDR) of 4.2%, and the peptide probability filter was 0.27% FDR. The identification of two unique peptides per protein was set as minimum for protein identification. Semiquantitative protein analysis was made based on Exponentially Modified Protein Abundance Index (emPAI) calculations, using no normalization and unpaired two-tailed Student *t* test.

Western Blot

Cells were lysed in RIPA lysis buffer containing 50 mmol/L Tris, 150 mmol/L NaCl, 1% Nonidet P-40, 0.5% sodium deoxycholate, 0.1% SDS, 1 mmol/L EDTA, and protease and phosphatase inhibitors. Cell lysate was incubated for 30 min at 4°C, followed by centrifugation at 16,900*g* for 15 min at 4°C. The protein concentration in the supernatant was determined, and Western blot and immunoprecipitation experiments were performed as described previously (19). Antibodies against the Cavβ1, β2, β3, and β4 were generated in-house (12,17,19). Other antibodies are as follows: anti-CREB (#4820) and anti–p-CREB (#9198) (Cell Signaling Technology); anti-MAFA (#NB400–137; Novus Biologicals); anti-IP_3R type 3 (IP_3R3 (#BD-610313; BD Biosciences); and anti-IP_3R3 (#AB9076; Merck).

Insulin Secretion

Pancreatic β-cells were plated and cultured in 24-well plates for 48 h. Next, cells were equilibrated for 1 h at 37°C and 5% CO_2 in Krebs-Ringer bicarbonate HEPES buffer (KRBH; 140 mmol/L NaCl, 3.6 mmol/L KCl, 2 mmol/L $NaHCO_3$, 2 mmol/L $CaCl_2$, 0.5 mmol/L NaH_2PO_4, 0.5 mmol/L $MgSO_4$, 10 mmol/L HEPES, 3 mmol/L glucose, and 0.1% [w/v] BSA, pH 7.4). The buffer was removed, and cells were incubated for 1 h at 37°C in KRBH containing 3 or 20 mmol/L glucose with or without nimodipine, xestospongin C, or vehicle, and insulin concentration in the supernatant was determined. For insulin content, cells were lysed in RIPA lysis buffer, and insulin content was determined. Insulin secretion and content were measured using the AlphaLISA Insulin Detection Kit (AL350; PerkinElmer).

Calcium Imaging

β-Cells were plated onto glass coverslips and loaded with 5 μmol/L Fura-2-AM (Invitrogen) for 45 min at 37°C. After loading, cells were washed twice with Tyrode's solution (140 mmol/L NaCl, 4 mmol/L KCl, 2 mmol/L $MgCl_2$, 10 mmol/L HEPES, and 10 mmol/L glucose, pH 7.4). Thereafter, glass coverslips were placed onto the stage of an inverted microscope equipped with a Fluar-20×/0.75 objective, a monochromator (polychrome V; TILL Photonics), and charge-coupled device camera (Andor Technology), which were controlled by TILLvisION software (TILL Photonics). Changes in intracellular calcium concentration ($[Ca^{2+}]$) were recorded during excitation at 340 and 380 nm every 2 s, and the emitted fluorescence was detected at >440 nm. Ratio images were calculated from images recorded at 340 and 380 nm after subtracting the background.

Electrophysiology

β-Cells were plated on glass coverslips, and whole-cell patch-clamp recordings were performed using a microscope equipped with a 40×-LD Achroplan objective (Zeiss), an EPC9 amplifier, and the PATCHMASTER software (HEKA Elektronik). Patch pipettes had resistances between 2 and 4 MΩ when filled with pipette solution (135 mmol/L CsCl, 3 mmol/L $MgCl_2$, 3 mmol/L Mg-ATP, 10 mmol/L EGTA, and 5 mmol/L HEPES, pH 7.4, with CsOH). The bath solution contained (102 mmol/L NaCl, 10 mmol/L $CaCl_2$, 5.4 mmol/L CsCl, 1 mmol/L $MgCl_2$, 20 mmol/L TEA-Cl, 5 mmol/L HEPES, and 10 mmol/L glucose, pH 7.4, with NaOH). After break-in, 50-ms voltage ramps spanning from −100 to +100 mV were applied every 2 s from a holding potential of −60 mV until the Cav currents reached a steady amplitude. Thereafter, voltage steps (400 ms) were applied every 2 s from a holding potential of −60 to +60 mV with 10-mV increments. All currents were normalized to the cell capacitance (pA/pF).

IP_3 Production Assay

β-Cells were plated and cultured in white opaque 384-well microplates for 24 h. Next, medium was discarded, and cells were stimulated with carbachol in the absence or presence of YM-254890 or U73122 for 30 min at 37°C. The IP_3 formation was measured as inositol monophosphate (IP_1) by the IP-One AlphaLISA Detection Kit (AL3145; PerkinElmer).

Data Analysis

Calcium and current recordings were analyzed by Igor Pro 6.02 (WaveMetrics). Graph presentations, curve fittings, statistics, and *P* values were obtained by Prism software (version 8.0.2; GraphPad). Data were tested for normality using D'Agostino-Pearson omnibus or Shapiro-Wilk normality tests. When normally distributed, data are reported as mean ± SD and otherwise as Tukey box and whiskers. For comparison of two groups, *P* values were calculated by the unpaired two-tailed Student *t* test or Mann-Whitney test. For three groups, one-way or two-way ANOVA with Bonferroni multiple-comparison or Kruskal–Wallis with Dunn multiple-comparison tests were used. Heat maps show the *z* scores of FPKM or emPAI values as indicated and were prepared by the "heatmap2" function from the gplots R package (https://cran.r-project.org/web/packages/gplots/).

Data and Resource Availability

The data sets generated during and/or analyzed during the current study are available from the corresponding author upon reasonable request.

RESULTS

Deletion of Cavβ3 Does Not Affect Cav Channel Activity in β-Cells

To investigate the role of Cavβ3 in pancreatic β-cells, we generated a Cavβ3-deficient β-cell line by CRISPR/Cas9-mediated targeting of the Cavβ3 gene *Cacnb3* (Fig. 1*A*). Sequencing identified a homozygous deletion of four nucleotides (CCTG), leading to a frameshift and premature STOP. Cavβ3 deletion was verified by Western blot using antibodies against different fragments of the Cavβ3 protein (Fig. 1*B*). Both antibodies detected the 55-kDa Cavβ3 protein in wild-type cells, which was absent in the Cavβ3-KO β-cells. Cavβ1 and Cavβ2 proteins, but not Cavβ4, were detectable, and their amounts were unaffected by the gene targeting (Fig. 1*C*).

Next, we assessed the function of Cav channels in these cells in the presence and absence of Cavβ3 protein. Whole-cell patch-clamp recordings revealed no significant differences in the Cav-current density (Fig. 2*A–C*). Application of verapamil (10 μmol/L) reduced mean maximal current densities by 59.97 ± 11.70 (wild-type) and 60.25 ± 7.19% (Cavβ3-KO) (Fig. 2*D–F*) and of nimodipine (2 μmol/L) by 21.87 ± 12.65 (wild-type) and 28.76 ± 17.28% (Cavβ3-KO) (Fig. 2*G–I*). Cav-current inhibition in both genotypes did not differ in the presence of verapamil ($P = 0.8887$) and nimodipine ($P = 0.1987$). In the presence of extracellular Ca^{2+}, depolarization induced by the addition of high potassium caused an immediate transient increase in intracellular [Ca^{2+}], which was significantly reduced in the presence of nimodipine (2 μmol/L) (Fig. 2*J* and Supplementary Fig. 1*A*). Peak amplitudes and area under the curve in response to high potassium in the presence or absence of nimodipine (2 μmol/L) did not differ between both genotypes (Fig. 2*J* and *K* and Supplementary Fig. 1). According to these data, Cav-channel function in β-cells is not dependent on Cavβ3, and the ratio of L-type to non–L-type current is not altered after Cavβ3 deletion.

RNA and Protein Profiling of Pancreatic β-Cells

Three independent RNA-sequencing experiments revealed 12,341 ± 13 and 12,394 ± 28 genes expressed with an FPKM value >1 in wild-type and Cavβ3-deficient cells. β-Cell–specific marker genes are expressed in Ins-1 β-cells, whereas the expression of marker genes for other pancreatic islet α-, δ-, or γ-cells (26,27) are barely detectable (Fig. 3*A*). About 10% of the genes were differentially expressed, with 14% of genes upregulated and 86% downregulated in the Cavβ3-deficient cells (Fig. 3*B* and Supplementary Table 1). Among them, genes encoding Insulin1 (*Ins1*), Insulin2 (*Ins2*), and genes associated with insulin signaling, including musculoaponeurotic fibrosarcoma oncogene homolog A (*Mafa*), Ca^{2+}/calmodulin–dependent protein kinase IV (*Camk4*), proprotein convertase subtilisin/kexin type-1 (*Pcsk1*), and nitric oxide synthase type-1 (*Nos1*) were upregulated, whereas thioredoxin-interacting protein (*Txnip*) and the vesicle-associated membrane protein-8 (*Vamp8*) were downregulated (Fig. 3*C*).

Genes encoding subunits of high voltage-gated Ca^{2+} channels were expressed (Fig. 3*D*), including *Cacnb1*, *b2*, and *b3* but not *Cacnb4*. *Cacnb3* was the most abundant β subunit (Fig. 3*D*). In the Cavβ3-deficient cells, *Cacnb3* transcripts were more than twofold reduced, probably due to enhanced degradation of nonsense transcripts after deletion of the four nucleotides in the targeted gene. Furthermore, several intracellular ion channels were expressed, such as IP_3R (*Itpr1*, *2*, and *3*), ryanodine receptors (*Ryr1*, *2*, and *3*), and two pore channels (*Tpcn1* and *Tpcn2*), without differences in expression levels in cells of either genotype (Fig. 3*D*).

Protein lysates from wild-type and Cavβ3-KO β-cells were analyzed by nanoflow liquid chromatography–tandem mass spectrometry, and 1,861 proteins were identified (Supplementary Table 2). Semiquantitative analysis calculating the emPAI revealed 63 proteins (~39%) with a more than twofold increase in Cavβ3-KO cells (Fig. 4*A*, left panel), whereas the amount of 103 proteins (~61%) were more than twofold reduced (Fig. 4*A*, right panel). In agreement with the transcriptome analysis (Fig. 3*B* and *C*), Insulin2, CaMKIV, and nitric oxide synthase-1 (NOS1)

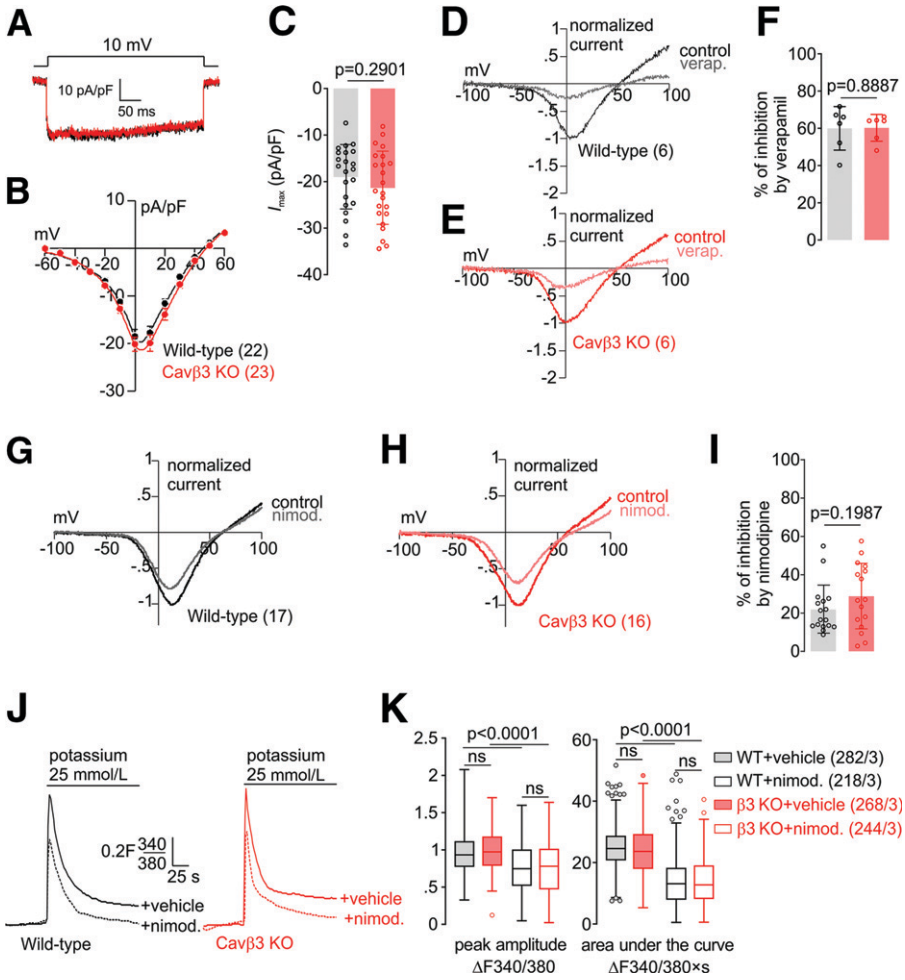

Figure 2—Voltage-gated Ca^{2+} currents and Ca^{2+} entry in wild-type and Cavβ3-KO β-cells. *A*: Whole cell currents in wild-type (black) and Cavβ3-KO (red) cells during a voltage step from a holding potential of −60 mV to 10 mV plotted vs. time. *B*: Current-voltage relationship obtained by voltage steps (400 ms) applied every 2 s from a holding potential of −60 mV up to +60 mV with 10-mV increments, shown as mean ± SEM of the maximal current amplitudes extracted at each voltage step. *C*: Maximal current amplitude (I_{max}) at 10 mV shown as single values (dot) and bar graph with mean ± SD. The number of cells included in the analysis is shown in *B*. Current-voltage relationships from wild-type (*D*) and Cavβ3-KO β-cells (*E*) obtained by 50-ms voltage ramps from −100 mV to +100 mV applied every 2 s from a holding potential of −60 mV before (control) and after the application of verapamil (verap.; 10 μmol/L) as indicated. *F*: Percentage of the Cav-current inhibition after application of verapamil analyzed from experiments in *D* and *E*. The number of cells included in the analysis are shown in *D* and *E*. Current-voltage relationships from wild-type (*G*) and Cavβ3-KO β-cells (*H*) obtained by 50-ms voltage ramps from −100 mV to +100 mV applied every 2 s from a holding potential of −60 mV before (control) and after the application of nimodipine (nimod.; 2 μmol/L) as indicated. *I*: Percentage of the Cav-current inhibition after application of nimodipine analyzed from experiments in *G* and *H*. Data in *F* and *I* are shown as single values and bar graph with mean ± SD, with the indicated *P* values calculated by unpaired two-tailed Student *t* test. *J*: Mean Fura-2 (F340/F380) ratiometric traces in the presence of 2 mmol/L extracellular Ca^{2+} before and after addition of 25 mmol/L potassium in wild-type (black) and Cavβ3-KO (red) cells. Cells were pretreated with 2 μmol/L nimodipine (+nimod., dashed lines) or vehicle (+vehicle, solid lines) for 10 min, and nimodipine was maintained during the whole experiment. *K*: Peak amplitude and the area under the curve of the potassium-induced Ca^{2+}-influx, shown as Tukey box and whiskers, with the boxes extending from the 25th to the 75th percentile and the line inside the box shows the median. The interquartile ranges represent the difference between the 25th and 75th percentiles. Whiskers are extended to the most extreme data point that is no more than 1.5 times the interquartile range from the edge of the box, and outliers beyond the whiskers are depicted as dots. The indicated *P* values were calculated by Kruskal–Wallis with Dunn multiple-comparisons test, and the number of measured cells (x) per experiment (y) are indicated as (x/y).

were significantly enhanced and VAMP8 tended to be decreased in Cavβ3-KO cells (Fig. 4*A* and *B*).

Elevated glucose concentrations have been shown to promote phosphorylation and activation of CREB via CaMKIV (28), which in turn induces *Mafa* and *Ins* expression (29). Accordingly, we analyzed phospho-CREB and MAFA protein levels in response to high glucose stimulation. CREB phosphorylation at Ser133 was detectable within a 1-minute incubation in the presence of 20 mmol/L glucose and was significantly enhanced in Cavβ3-KO cells (Fig. 4*C* and *D*). In addition, the amount of MAFA protein was increased in Cavβ3-KO cells before

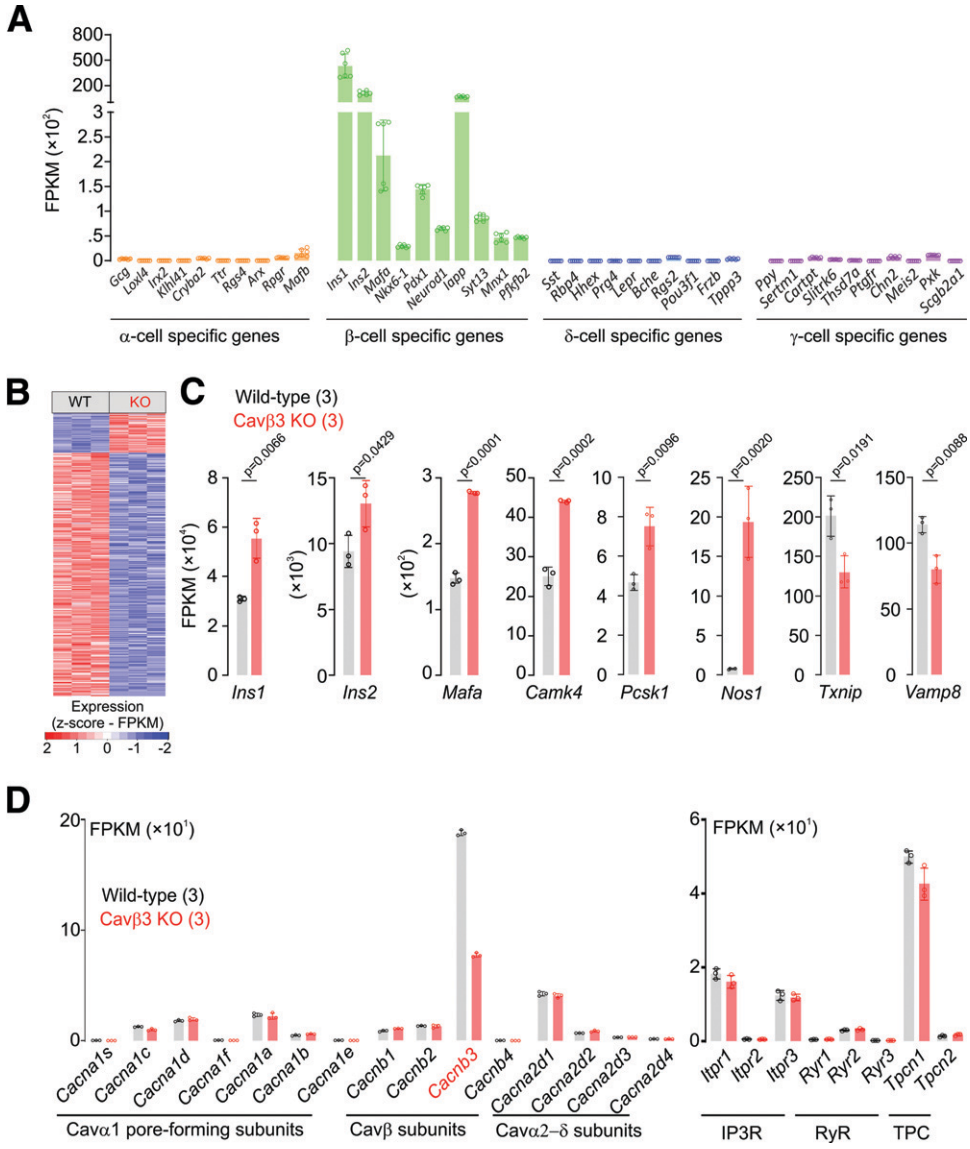

Figure 3—RNA profiling of pancreatic β-cells in the presence (wild-type) and absence (KO) of Cavβ3. *A*: Expression levels of pancreatic α-, β-, δ-, and γ-cell-specific genes in wild-type and Cavβ3-KO (n = 6) Ins-1 cells. Data are shown as single values of FPKM and bar graphs with mean ± SD. *B*: Differentially expressed genes identified by RNA sequencing in wild-type (WT; n = 3) and Cavβ3-KO (KO; n = 3) β-cells with an FDR-adjusted P value <0.05. *C*: Expression levels of *Ins1*, *Ins2*, *Mafa*, *Camk4*, *Pcsk1*, *Nos1*, *Txnip*, and *Vamp8* genes from WT (black; n = 3) and Cavβ3-KO (red; n = 3) cells, shown as single FPKM values and bar graphs with mean ± SD, with the indicated P values calculated by unpaired two-tailed Student t test. *D*: Gene expression levels of high voltage-gated Ca^{2+} channel subunits and of intracellular ion channels obtained by RNA sequencing from WT (black; n = 3) and Cavβ3-KO (red; n = 3) cells, shown as single FPKM values and bar graphs with mean ± SD.

and after exposure to glucose. These findings indicate that Cavβ3 fine-tunes the CaMKIV/CREB-dependent transcription.

Glucose-Induced Insulin Secretion in the Absence or Presence of Cavβ3

Next, we evaluated the impact of *Cacnb3* gene deletion on glucose-induced insulin secretion (GIIS) and insulin content in pancreatic β-cells. Wild-type and Cavβ3-KO cells were exposed to low (3 mmol/L) and high (20 mmol/L) glucose concentrations, and insulin release was subsequently determined. Insulin release in the presence of both low and high extracellular glucose concentrations and insulin content were significantly enhanced in Cavβ3-KO cells (Fig. 5*A* and *B*). Inhibition of L-type Cav channels by nimodipine (Fig. 5*C*) or of IP_3Rs by xestospongin C (Fig. 5*D*) resulted in a significant reduction of insulin secretion in both genotypes, suggesting that GIIS in β-cells depends on the activity of L-type Cav channels and IP_3Rs.

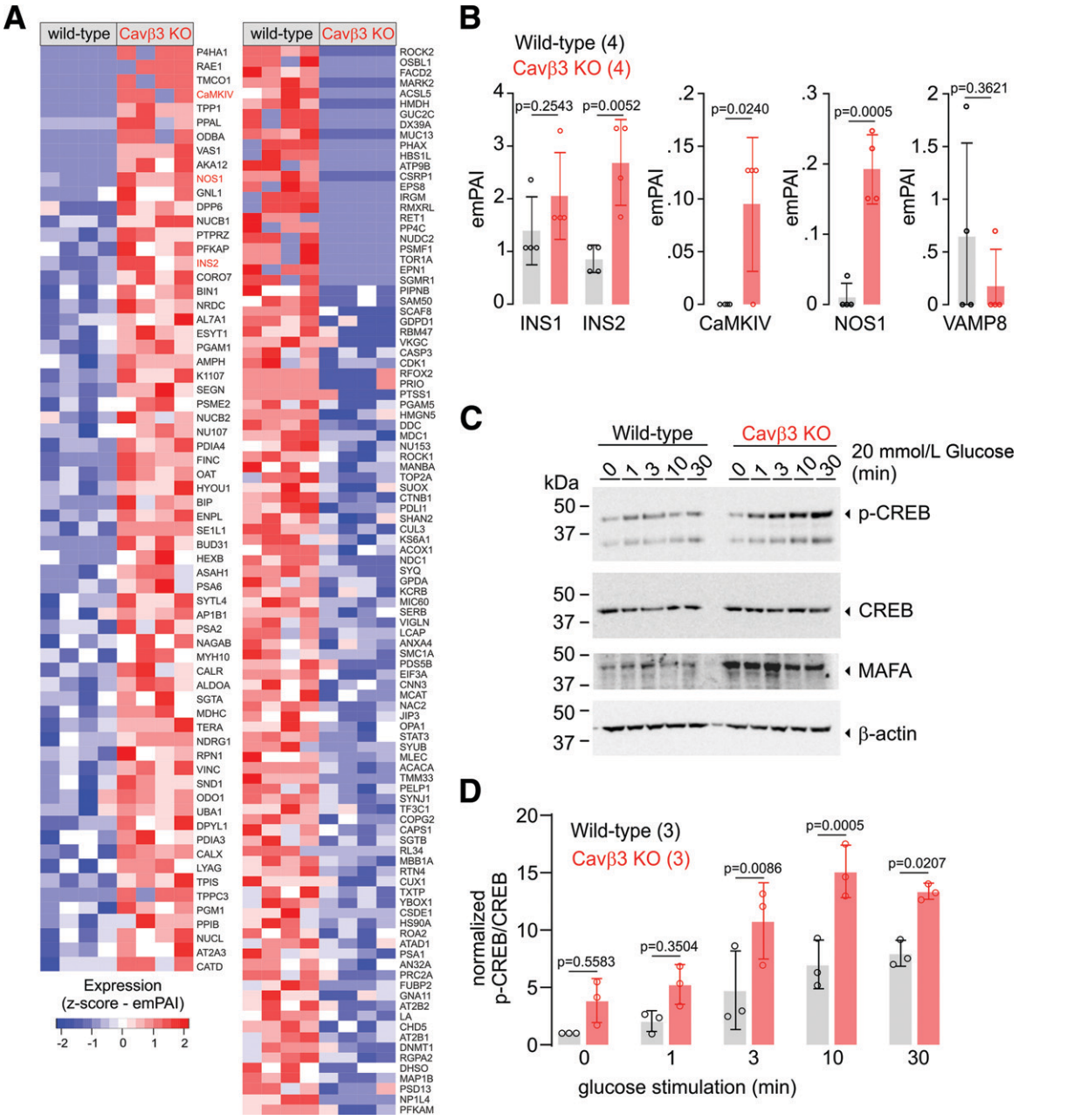

Figure 4—Protein profiling of pancreatic β-cells in the presence (wild-type) and absence (KO) of Cavβ3. *A*: Protein abundances identified by mass spectrometry, upregulated (66 proteins, left panel) and downregulated (103 proteins, right panel) in Cavβ3-KO compared with the wild-type β-cells (identified based on the emPAI values with a *P* value <0.05, calculated by unpaired two-tailed Student *t* test) ($n = 4$: three biological replicates and one technical replicate). *B*: Protein levels of INS1, INS2, CaMKIV, NOS1, and VAMP8 shown as single emPAI values and bar graphs with mean ± SD, with the indicated *P* values calculated by unpaired two-tailed Student *t* test. *C*: Western blot of protein extracts from wild-type and Cavβ3-KO cells (50 μg protein/lane) using specific antibodies against the phosphorylated form of CREB (p-CREB), total CREB, MAFA, and β-actin as indicated. Cells were stimulated with KRBH buffer containing 20 mmol/L glucose for 1, 3, 10, and 30 min or left untreated (0). *D*: Densitometric quantification of the antibody stain showing the p-CREB/CREB ratio obtained from three Western blots running protein lysates obtained from independent β-cell cultures. Data are shown as single values and bar graphs with mean ± SD, with the indicated *P* values calculated using two-way ANOVA followed by Bonferroni multiple-comparison test.

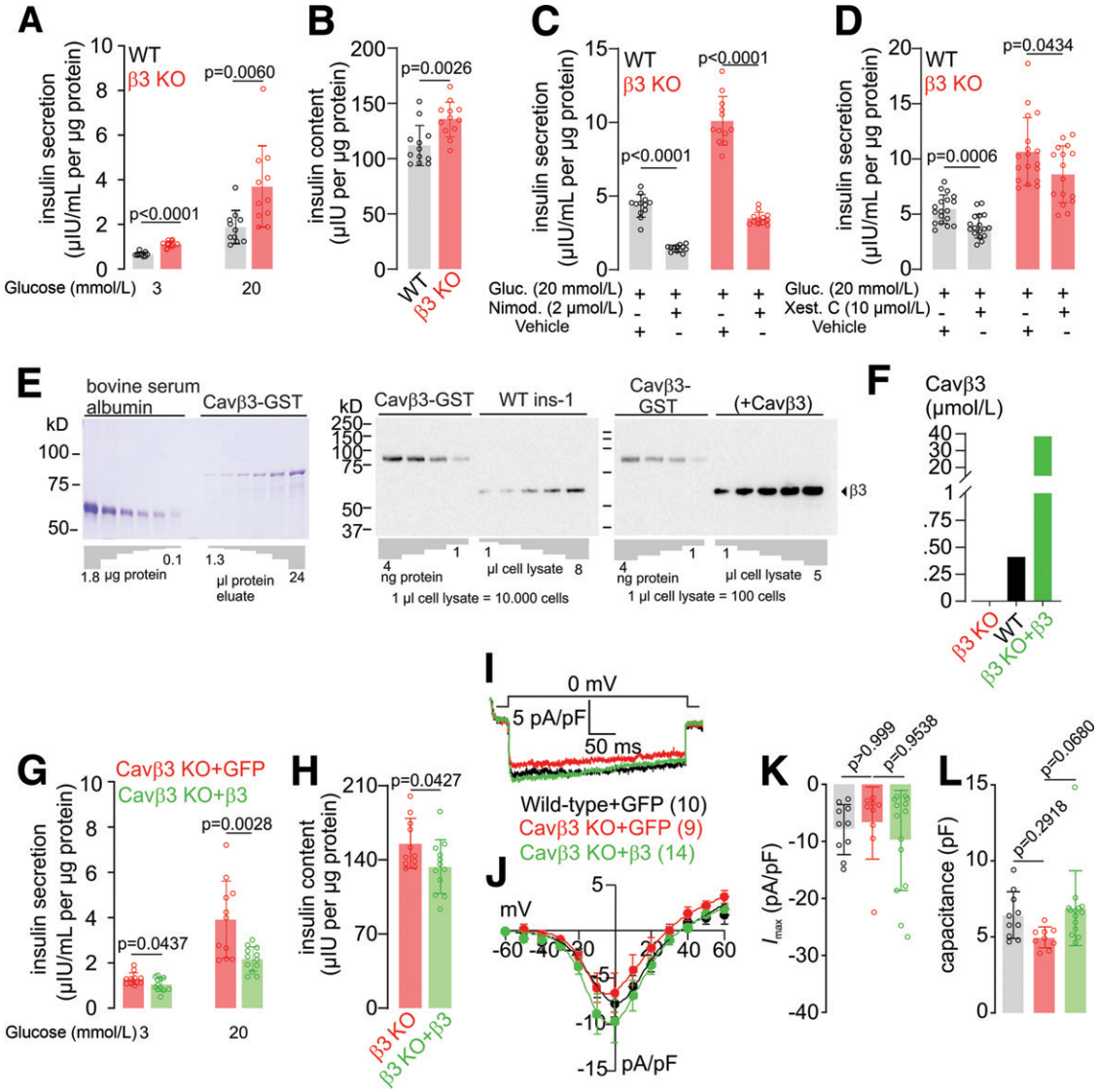

Figure 5—The Cavβ3 protein decreases insulin secretion in a dose-dependent manner without affecting the Cav channel function. Glucose-dependent (3 mmol/L and 20 mmol/L) insulin secretion (*A*) and total insulin content (*B*) normalized to total cellular protein content measured from wild-type (WT; black) and Cavβ3-KO (β3 KO; red) β-cells shown as single values and bar graphs with mean ± SD, with the indicated *P* values calculated by unpaired two-tailed Student *t* test. Insulin secretion normalized to total cellular protein content measured from wild-type (black) and Cavβ3-KO (red) β-cells exposed to 20 mmol/L glucose (Gluc.) in the absence or presence of nimodipine (Nimod.; 2 µmol/L) (*C*) or xestospongin C (Xest. C; 10 µmol/L) (*D*). Data are shown as single values and bar graphs with mean ± SD, with the indicated *P* values calculated by unpaired two-tailed Student *t* test. *E*: Estimation of the Cavβ3 protein concentration in β-cells. The concentration of recombinant GST-Cavβ3 was determined by densitometric analysis relative to the known concentrations of BSA (left) in Coomassie-stained SDS-PAGE. Immunostain intensities obtained from anti-Cavβ3 Western blots from known amounts of recombinant GST-Cavβ3 protein (1, 2, 3, and 4 ng) were compared with endogenous Cavβ3 protein of a defined number of wild-type β-cells (middle) and Cavβ3-KO β-cells transfected with the *Cacnb3* cDNA (+Cavβ3, right). Transfected cells were identified by their green fluorescence and sorted by preparative FACS before analyses. Cavβ3 is estimated at 36.8 fg/single wild-type β-cell and 3.4 pg/single Cavβ3-cDNA–expressing cell. *F*: Considering the β-cell volume of 1.6 pL, Cavβ3 protein concentrations were calculated as 0.41 µmol/L in wild-type cells and as 38.6 µmol/L per cell after transfection with the Cavβ3 cDNA. Glucose-dependent (3 mmol/L and 20 mmol/L) insulin secretion (*G*) and total insulin content (*H*) normalized to total cellular protein content measured from Cavβ3-KO cells transfected with either IRES-GFP (Cavβ3 KO+GFP; red) or Cavβ3-IRES-GFP (Cavβ3 KO+β3; green) cDNA shown as single values and bar graphs with mean ± SD, with the indicated *P* values calculated by unpaired two-tailed Student *t* test. Note: insulin release and content are overestimated in β3 KO+β3 cells, a mixture of transfected and nontransfected cells. *I*: Whole cell currents during voltage steps from a holding potential of −60 mV to 0 mV plotted vs. time recorded from wild-type cells (black, transfected with IRES-GFP as a control) or Cavβ3-KO cells transfected with IRES-GFP (red) or with Cavβ3-IRES-GFP (green). *J*: Current-voltage relationships obtained by voltage steps (400 ms) applied every 2 s from a holding potential of −60 mV up to +60 mV with 10-mV increments shown as mean ± SEM of the maximal current amplitudes extracted at each voltage step. *K* and *L*: Maximal current amplitude (I_{max}) at 0 mV and cell capacitance shown as single values and bar graphs with mean ± SD, with the indicated *P* values calculated by one-way ANOVA followed by Bonferroni multiple-comparison test. The number of cells analyzed in *I*–*L* is indicated in *I*.

To investigate whether modulation of insulin release depends on the amount of Cavβ3 protein present in the cells, Cavβ3 protein concentrations were determined in wild-type cells and cells overexpressing the Cavβ3 cDNA. By relating the amount of Cavβ3 protein of a defined number of β-cells with a defined amount of Coomassie-stained recombinant Cavβ3 protein (Fig. 5*E*), we estimated an amount of 36.8 fg Cavβ3 protein per single wild-type β-cell and of 3.4 pg per single Cavβ3-cDNA overexpressing β-cell. With regard to the cell's capacitance of 6.66 ± 0.42 pF (Fig. 5*L*) and considering a specific capacitance of ∼1 μF/cm^2 (30,31) and the cell to be a sphere, we calculated the volume of a single cell as ∼1.6 pL. From these calculations, we end up with an estimated Cavβ3 protein concentration of 0.41 μmol/L in wild-type and 38.6 μmol/L in cells after transfection with the Cavβ3 cDNA (Fig. 5*F*). Compared with Cavβ3-KO cells, GIIS in response to low and high glucose and total cellular insulin content were reduced in the presence of Cavβ3 (Fig. 5*G* and *H*). In contrast, neither the mean maximal Cav-current density nor the cell capacitance showed significant differences in the presence or absence of Cavβ3 (Fig. 5*I–L*).

Cytosolic Ca^{2+} Signaling Is Modulated by Cavβ3 in Pancreatic β-Cells

The initiation of the CaMKIV/CREB signaling pathway depends on cytoplasmic [Ca^{2+}], and we addressed the effect of Cavβ3 on intracellular Ca^{2+} signaling in β-cells. In the presence of extracellular Ca^{2+}, application of low (3 mmol/L) or high (17 mmol/L) concentrations of glucose evoked Ca^{2+} oscillations in β-cells (Fig. 6*A* and Supplementary Fig. 2*A*). Deletion of Cavβ3 resulted in a significant increase in the frequency of Ca^{2+} oscillations induced by low and high glucose and in the peak amplitude of Ca^{2+} oscillations induced by glucose at 17 mmol/L but not at 3 mmol/L glucose (Fig. 6*B* and Supplementary Fig. 2*B*). Conversely, *Cacnb3* overexpression in Cavβ3-deficient β-cells reduced the frequency and the peak amplitude of glucose-induced Ca^{2+} oscillations (Fig. 6*C* and *D*). Pretreatment with xestospongin C significantly reduced the frequency and peak amplitude of glucose-induced Ca^{2+} oscillations (Supplementary Fig. 2*C* and *D*), indicating the involvement of IP_3Rs. To understand the way in which Cavβ3 influences glucose-induced Ca^{2+} oscillations, IP_3-dependent Ca^{2+} release was determined. Pancreatic β-cells express the *Chrm3* gene (Supplementary Table 1) (32) encoding the muscarinic M3 receptor. After administration of carbachol, phospholipase C is activated via $G\alpha_{q/11}$, and IP_3 and diacylglycerol are formed. IP_3 binds to the IP_3R and initiates Ca^{2+} release. In the absence of extracellular Ca^{2+}, the peak amplitude and area under the curve were significantly increased in Cavβ3-KO cells (Fig. 7*A* and *B*) and decreased after Cavβ3-cDNA expression (Fig. 7*C* and *D*). Next, the accumulation of IP_1, a stable downstream metabolite of IP_3, was measured in

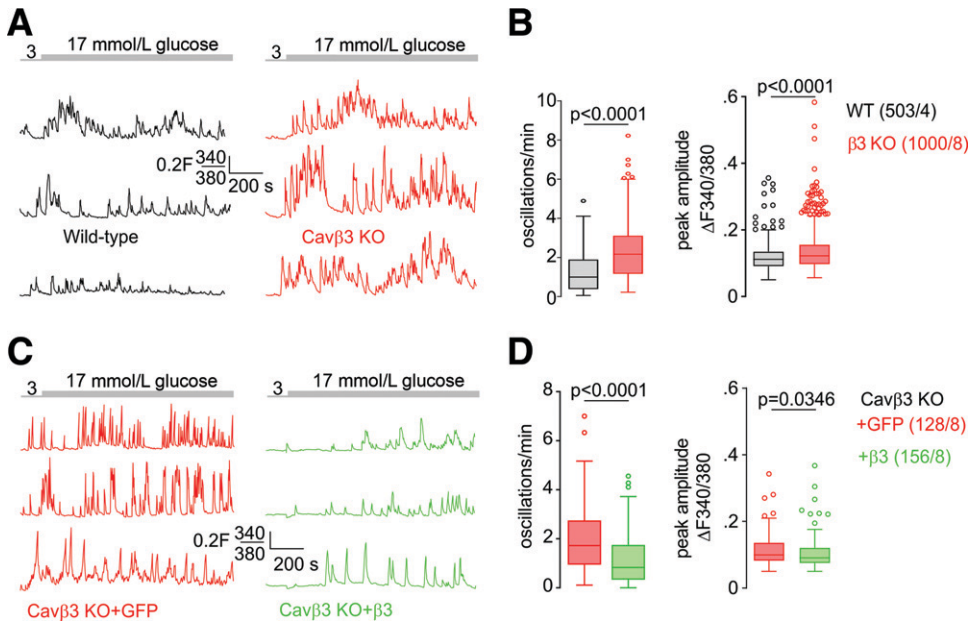

Figure 6—Cavβ3 inhibits frequency of glucose-induced Ca^{2+} oscillations. Representative Fura-2 (F340/380) ratiometric traces in the presence of extracellular Ca^{2+} from wild-type (WT; black) and Cavβ3-KO (red) β-cells (*A*) or from Cavβ3-KO β-cells transfected with either IRES-GFP (red) or Cavβ3-IRES-GFP (green) (*C*) in the presence of 3 mmol/L and 17 mmol/L extracellular glucose as indicated. *B* and *D*: Numbers of glucose-evoked Ca^{2+} oscillations per minute (left) and mean peak amplitude per cell (right) from experiments in *A* and *C*. Data in *B* and *D* are shown as Tukey box and whiskers with the boxes extending from the 25th to the 75th percentile, and the line inside the box shows the median. The interquartile ranges represent the difference between the 25th and 75th percentiles. Whiskers are extended to the most extreme data point that is no more than 1.5 times the interquartile range from the edge of the box, and outliers beyond the whiskers are depicted as dots. The indicated *P* values were calculated by Mann-Whitney test, and the number of measured cells (x) per experiment (y) are indicated as (x/y).

response to carbachol stimulation in the absence or presence of the $G\alpha_{q/11}$-specific inhibitor YM-254890 or the phospholipase C inhibitor U73122 (Fig. 7*E*). Carbachol substantially increased the IP_3 formation, and this effect was antagonized by YM-254890 or U73122. IP_3 formation was not significantly different in β-cells of both genotypes, before and after addition of carbachol (Fig. 7*E*). To determine the total amount of Ca^{2+} that can be mobilized from intracellular stores, β-cells in the absence of extracellular calcium were treated sequentially with thapsigargin plus

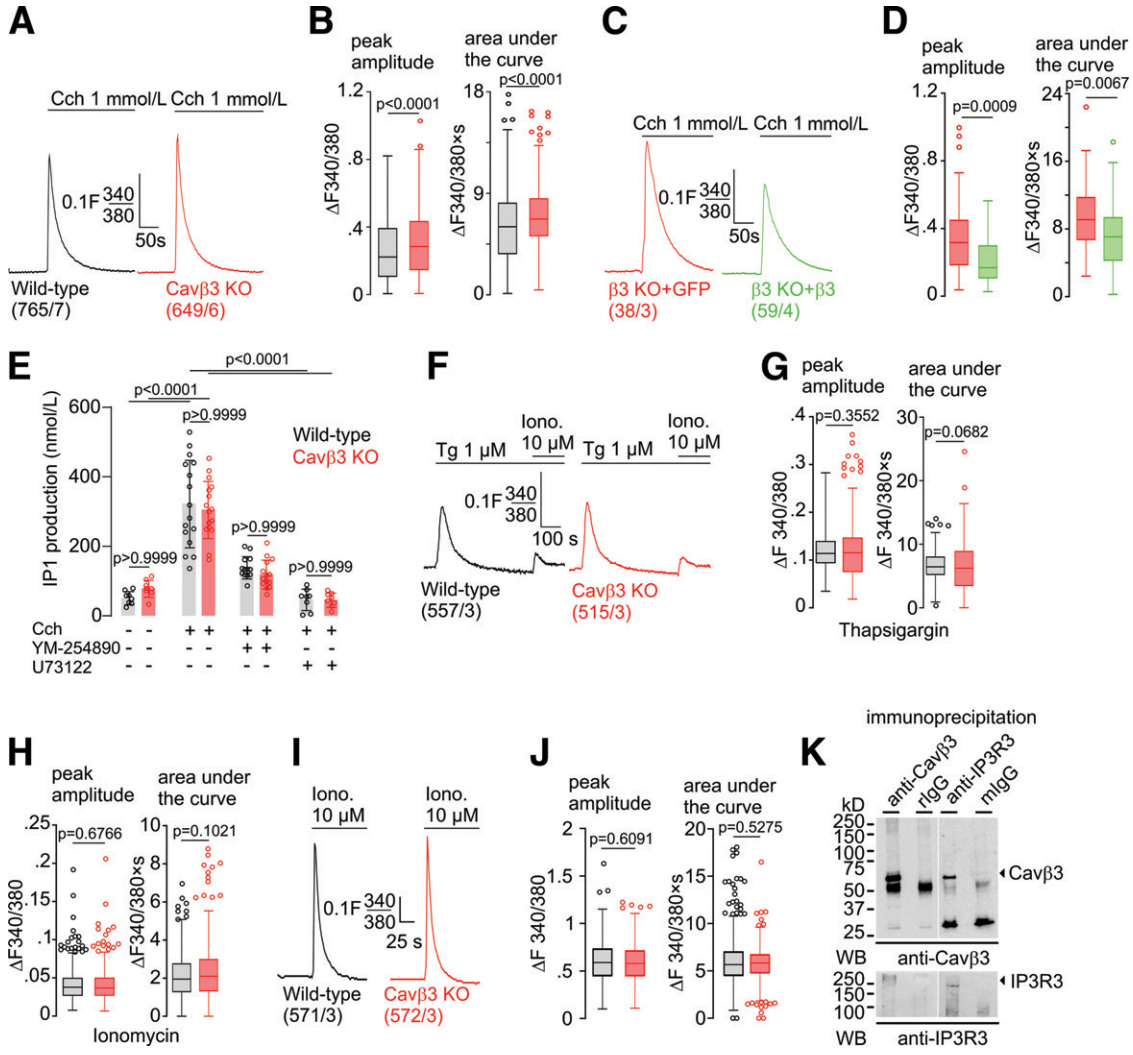

Figure 7—Cavβ3 binds to the IP_3 receptor and inhibits IP_3-dependent Ca^{2+} release. Mean Fura-2 (F340/380) ratiometric traces in the absence of extracellular Ca^{2+} from wild-type (black) and Cavβ3-KO β-cells (red) (*A*) and from Cavβ3-KO β-cells transfected with either IRES-GFP (red) or Cavβ3-IRES-GFP (green) (*C*) before and after application of carbachol (Cch; 1 mmol/L). *B* and *D*: Peak amplitude (left) and the area under the curve (right) of carbachol-evoked Ca^{2+} signals from experiments shown in *A* and *C*. *E*: IP_3 production as measured by the accumulation of IP_1 (in nanomoles per liter) in wild-type (black) and Cavβ3-KO β-cells (red) in response to carbachol stimulation in the absence or presence of the $G\alpha_{q/11}$-specific inhibitor YM-254890 (100 nmol/L) or the phospholipase C inhibitor U73122 (10 μmol/L). Data are shown as single values and bar graphs with mean ± SD, with the indicated *P* values calculated by one-way ANOVA followed by Bonferroni multiple-comparison test. *F*: Mean Fura-2 (F340/380) ratiometric traces in the absence of extracellular Ca^{2+} from wild-type (black) and Cavβ3-KO (red) β-cells before and after application of thapsigargin (Tg; 1 μmol/L) and then ionomycin (Iono.; 10 μmol/L). Peak amplitude (left) and area under the curve (right) of thapsigargin (*G*) and ionomycin-evoked (*H*) Ca^{2+} signal. *I*: Mean Fura-2 (F340/380) ratiometric traces in the absence of extracellular Ca^{2+} from wild-type (black) and Cavβ3-KO (red) β-cells before and after application of ionomycin (10 μmol/L). *J*: Peak amplitude and area under the curve of ionomycin-evoked Ca^{2+} signal. Data in *B*, *D*, *G*, *H*, and *J* are shown as Tukey box and whiskers with the boxes extend from the 25th to the 75th percentile, and the line inside the box shows the median. The interquartile ranges represent the difference between the 25th and 75th percentiles. Whiskers are extended to the most extreme data point that is no more than 1.5 times the interquartile range from the edge of the box, and outliers beyond the whiskers are depicted as dots. The indicated *P* values were calculated by Mann-Whitney test, and the number of measured cells (x) per experiment (y) are indicated as (x/y). *K*: Coimmunoprecipitation of Cavβ3 and the IP_3R3. Immunoprecipitations were performed with antibodies against Cavβ3, nonspecific rabbit Ig (rIgG), anti-IP_3R3, and nonspecific mouse Ig (mIgG). Eluted protein complexes were subjected to Western blot (WB) using anti-Cavβ3 (top blot) and anti-IP_3R3 (bottom blot).

ionomycin (Fig. 7*F*) or ionomycin alone (Fig. 7*I*). The peak amplitudes of the thapsigargin- and ionomycin-triggered Ca^{2+} signals and the areas under the traces (curves) did not differ between the two genotypes (Fig. 7*G*, *H*, and *J*), suggesting that the calcium content in intracellular stores is not affected by the Cavβ3 protein. The transcript levels of $IP_3R1–3$ also did not differ in cells of both genotypes (Fig. 3*D*). Using an antibody for the IP_3R3, the Cavβ3 protein was coimmunoprecipitated with IP_3R3 in β-cells and vice versa (Fig. 7*K* and Supplementary Fig. 2*E*). These experiments suggest that Cavβ3 binds to the IP_3R and interferes with IP_3- and glucose-dependent Ca^{2+} signaling. This is consistent with our results in fibroblasts isolated from mouse tissue, which support that the Cavβ3 protein reduces the sensitivity of cells to low IP_3 levels via interaction with the IP_3R (19).

DISCUSSION

RNA sequencing of rat pancreatic β-cells revealed the expression of genes encoding high voltage-gated Ca^{2+} channel subunits (Fig. 3*D*). In the endocrine pancreas, a rise in $[Ca^{2+}]$ mediates insulin secretion, and it was shown that in human and mouse pancreatic β-cells, the Cav1.2 and Cav1.3 in particular contribute to Ca^{2+} influx. Mutations in the genes encoding the ion-conducting pores of these channels led to alterations in whole-cell Ca^{2+} currents, insulin secretion, and systemic glucose tolerance (13,33,34). Following genetic deletion of the *Cacna2d1* gene, Cav currents, insulin release, and β-cell mass were decreased, leading to glucose intolerance (16).

In contrast, genetic ablation of Cavβ3 increased insulin secretion and glucose clearance without affecting Cav currents in β-cells (17,18). In these studies, the *Cacnb3* gene was deleted in the whole animal and not specifically in pancreatic β-cells. Therefore, it cannot be excluded that ablation of Cavβ3 not only in pancreatic β-cells contributes to the observed phenotype. To investigate the function of the *Cacnb3* gene and its effects in pancreatic β-cells alone, we deleted the *Cacnb3* gene in pancreatic β-Ins-1 cells by CRISPR/Cas9 (Fig. 1*A*)

In Cavβ3-KO cells, GIIS, insulin content, Ca^{2+} release, and the frequency of Ca^{2+} oscillations were increased compared with wild-type cells, but the whole Cav currents and the ratio of L-type to non-L-type currents remained unchanged (Figs. 2 and 5). When the amount of Cavβ3 was increased above the concentration level in wild-type cells, the effects on GIIS, insulin content, and Ca^{2+} signaling were even more reversed, without Cav channel function being affected (Fig. 5). Taken together, these results argue for a cell-autonomous mechanism in which the absence of Cavβ3 in β-cells alone is responsible for the effects on insulin release and that these effects of Cavβ3 are independent of its function as a Cav channel subunit.

Jeon et al. (35) identified Cavβ3 and characterized its function in hippocampal CA1 pyramidal neurons. After deletion of the *Cacnb3* gene, Cav currents remain unchanged in these cells. At the same time, *N*-methyl-D-aspartate receptor–mediated synaptic currents were increased (35). We showed that deletion of *Cacnb3* gene increased the sensitivity of fibroblasts to low concentrations of IP_3 without affecting Cav currents (19,20).

RNA profiling revealed that in rat β-cells, among all Cav subunit–encoding genes, the Cavβ3 was the most highly expressed, >10-fold higher than the genes of Cavβ1 and Cavβ2 (Fig. 3*D*). The transcription levels of these genes do not differ in wild-type and Cavβ3-KO cells, so Cavβ2 and Cavβ1 could function as subunits of Cav1 channels in these cells. The *Cacnb4* gene was detected with FPKM values <1 in both genotypes and in Western blot Cavβ4 protein was not detectable because the protein was either not present in these cells or the sensitivity of the antibodies was not sufficient to detect it (Figs. 1*C* and 3*D*).

Significantly upregulated in Cavβ3-KO cells are genes associated with insulin transcription, including *Ins1* and *Ins2*. While the rat and mouse genomes contain two insulin genes, only a single insulin gene exists in the human genome, which is homologous to the rodent *Ins2* gene (36). The proteomic data support the transcriptomic data: they show a significant increase in insulin, NOS1, CaMKIV, CREB, and MAFA (Fig. 4). CaMKIV plays a role in CREB activation, which in turn contributes to *Mafa* and *Ins* expression (28,29,37). Expression of a constitutively active CaMKIV mutant in β-Ins-1 cells enhanced glucose-induced *Insulin* gene expression, while a dominant-negative mutant of this protein repressed insulin promoter activity (38). The transcription factor *Mafa*, which regulates glucose-dependent transcription of insulin, is dependent on the CREB pathway (29) and is considered a sensor of pancreatic β-cell activity (39). The significantly higher glucose-dependent CREB phosphorylation and concomitant increase in MAFA protein levels in Cavβ3-KO β-cells (Fig. 4*C* and *D*) suggest that Cavβ3 in wild-type cells modulates *Insulin* transcription via a CaMKIV/CREB-dependent pathway.

Txnip inhibits insulin production by downregulating *Mafa* (40), while *Txnip* gene deficiency prevents β-cell apoptosis (41). In Cavβ3-KO β-cells, *Txnip* transcripts are significantly reduced compared with wild-type cells (Fig. 3*B* and *C*). This reduction could protect β-cells from the stress caused by increased glucose-dependent insulin production. VAMP8 mediates the recruitment of insulin granules to the plasma membrane (42). Deletion of the *Vamp8* gene in mice leads to an increase in insulin sensitivity and changes in glucose clearance depending on the genetic background (42–44). Transcripts of *Vamp8* are decreased in Cavβ3-KO β-cells compared with wild-type cells (Fig. 3*B* and *C*), possibly counteracting the increased insulin transcription and release. The transcript levels of *Nos1* and *Pcsk1* are significantly increased in Cavβ3-KO β-cells and may additionally contribute to the increased insulin release in Cavβ3-KO β-cells. Thus, the formation

of NO is associated with increased GIIS (45), and a defect in PCSK1, which converts proinsulin into an active hormone, has been linked to obesity (46).

In addition to Ca^{2+} influx into the β-cell via Cav channels, the release of Ca^{2+} from intracellular stores also influences the regulation of insulin secretion and glucose homeostasis. For example, knockin mice with RyR2 mutations, discovered in humans with a genetic form of exercise-induced sudden cardiac death, show glucose intolerance. The mutation results in intracellular Ca^{2+} leak through RyR2 channels (7). Another mutation that occurred spontaneously in a mouse colony results in a genomic deletion of two exons in *Itpr1* and aberrant splicing of *Itpr1* mRNA transcripts (47). Animals heterozygous for this mutation show glucose intolerance, reduced β-cell mass, and reduced pancreatic islet insulin content (48). Single nucleotide polymorphisms in the *ITPR3* gene are associated with type 1 diabetes in humans (49,50).

In the β-cells studied in this report, IP_3- and glucose-dependent Ca^{2+} signaling are decreased in the presence of Cavβ3 (Figs. 6 and 7). Cavβ3 interacts directly with IP_3R3 and negatively affects *Insulin* gene expression, insulin content, and secretion. In contrast, in the absence of Cavβ3, *Insulin* transcription and secretion are increased.

Acknowledgments. The authors thank Christine Wesely, Oliver Glaser, Armin Weber, and Martin Simon-Thomas (Institut für Experimentelle und Klinische Pharmakologie und Toxikologie, Homburg, Germany) for the excellent technical assistance. Ins-1 cells were generously provided by Prof. Per-Olof Berggren and Dr. Barbara Leibiger (Karolinska Institutet, Stockholm, Sweden).

Funding. The study was funded by the Deutsche Forschungsgemeinschaft CRC 894 (to A. Beck, S.E.P., V.F., and A.Bel.).

Duality of Interest. No potential conflicts of interest relevant to this article were reported.

Author Contributions. A.Bec. and S.E.P. generated the Cavβ3-KO β-(Ins-1) cells using CRISPR/Cas9. B.W. and A. Beck performed patch-clamp experiments. H.S., M.A., D.M., and A.Bel. performed Ca^{2+}-imaging experiments. A.Bel. performed insulin secretion, IP3 production, and Western blot experiments and together with Q.S. analyzed the RNA-sequencing data. C.F.-T. performed mass spectrometry experiments. A.Bel. wrote the original draft of manuscript. C.F.-T., A. Beck, and S.E.P. edited the manuscript. V.F. and A.Bel. conceived all experiments and contributed to all aspects of the manuscript, funding, and supervision and wrote the manuscript. A.Bel. is the guarantor of this work and, as such, had full access to all of the data in the study and takes responsibility for the integrity of the data and the accuracy of the data analysis.

References

1. Ashcroft FM, Rorsman P. Electrophysiology of the pancreatic beta-cell. Prog Biophys Mol Biol 1989;54:87–143

2. Grapengiesser E, Gylfe E, Hellman B. Glucose-induced oscillations of cytoplasmic Ca2+ in the pancreatic beta-cell. Biochem Biophys Res Commun 1988;151:1299–1304

3. Henquin JC, Meissner HP. Significance of ionic fluxes and changes in membrane potential for stimulus-secretion coupling in pancreatic B-cells. Experientia 1984;40:1043–1052

4. Kindmark H, Köhler M, Efendić S, Rorsman P, Larsson O, Berggren PO. Protein kinase C activity affects glucose-induced oscillations in cytoplasmic free Ca2+ in the pancreatic B-cell. FEBS Lett 1992;303:85–90

5. Srivastava M, Atwater I, Glasman M, et al. Defects in inositol 1,4,5-trisphosphate receptor expression, Ca^{2+} signaling, and insulin secretion in the anx7(+) knockout mouse. Proc Natl Acad Sci USA 1999;96:13783–13788

6. Tamarina NA, Kuznetsov A, Rhodes CJ, Bindokas VP, Philipson LH. Inositol (1,4,5)-trisphosphate dynamics and intracellular calcium oscillations in pancreatic beta-cells. Diabetes 2005;54:3073–3081

7. Santulli G, Pagano G, Sardu C, et al. Calcium release channel RyR2 regulates insulin release and glucose homeostasis. J Clin Invest 2015;125:1968–1978

8. Hofmann F, Flockerzi V, Kahl S, Wegener JW. L-type CaV1.2 calcium channels: from in vitro findings to in vivo function. Physiol Rev 2014;94:303–326

9. Kharade SV, Sonkusare SK, Srivastava AK, et al. The β3 subunit contributes to vascular calcium channel upregulation and hypertension in angiotensin II-infused C57BL/6 mice. Hypertension 2013;61:137–142

10. Kazim AS, Storm P, Zhang E, Renström E. Palmitoylation of Ca^{2+} channel subunit $Ca_V\beta_{2a}$ induces pancreatic beta-cell toxicity via Ca^{2+} overload. Biochem Biophys Res Commun 2017;491:740–746

11. Yang L, Katchman A, Kushner J, et al. Cardiac CaV1.2 channels require β subunits for β-adrenergic-mediated modulation but not trafficking. J Clin Invest 2019;129:647–658

12. Meissner M, Weissgerber P, Londoño JE, et al. Moderate calcium channel dysfunction in adult mice with inducible cardiomyocyte-specific excision of the cacnb2 gene. J Biol Chem 2011;286:15875–15882

13. Schulla V, Renström E, Feil R, et al. Impaired insulin secretion and glucose tolerance in beta cell-selective Ca(v)1.2 Ca^{2+} channel null mice. EMBO J 2003;22:3844–3854

14. Jing X, Li DQ, Olofsson CS, et al. CaV2.3 calcium channels control second-phase insulin release. J Clin Invest 2005;115:146–154

15. Matsuda Y, Saegusa H, Zong S, Noda T, Tanabe T. Mice lacking Ca(v)2.3 (alpha1E) calcium channel exhibit hyperglycemia. Biochem Biophys Res Commun 2001;289:791–795

16. Mastrolia V, Flucher SM, Obermair GJ, et al. Loss of $\alpha_2\delta$-1 calcium channel subunit function increases the susceptibility for diabetes. Diabetes 2017;66:897–907

17. Berggren PO, Yang SN, Murakami M, et al. Removal of Ca^{2+} channel beta3 subunit enhances Ca2+ oscillation frequency and insulin exocytosis. Cell 2004;119:273–284

18. Lee K, Kim J, Köhler M, et al. Blocking Ca^{2+} channel β_3 subunit reverses diabetes. Cell Rep 2018;24:922–934

19. Belkacemi A, Hui X, Wardas B, et al. IP_3 receptor-dependent cytoplasmic Ca^{2+} signals are tightly controlled by Cavβ3. Cell Rep 2018;22:1339–1349

20. Belkacemi A, Laschke MW, Menger MD, Flockerzi V. Scratch migration assay and dorsal skinfold chamber for in vitro and in vivo analysis of wound healing. J Vis Exp 2019;151:e59608. DOI: 10.3791/59608

21. Becker A, Mannebach S, Mathar I, et al. Control of insulin release by transient receptor potential melastatin 3 (TRPM3) ion channels. Cell Physiol Biochem 2020;54:1115–1131

22. Ran FA, Hsu PD, Wright J, Agarwala V, Scott DA, Zhang F. Genome engineering using the CRISPR-Cas9 system. Nat Protoc 2013;8:2281–2308

23. Heigwer F, Kerr G, Boutros M. E-CRISP: fast CRISPR target site identification. Nat Methods 2014;11:122–123

24. Bae S, Park J, Kim JS. Cas-OFFinder: a fast and versatile algorithm that searches for potential off-target sites of Cas9 RNA-guided endonucleases. Bioinformatics 2014;30:1473–1475

25. Fecher-Trost C, Wissenbach U, Beck A, et al. The in vivo TRPV6 protein starts at a non-AUG triplet, decoded as methionine, upstream of canonical initiation at AUG. J Biol Chem 2013;288:16629–16644

26. Muraro MJ, Dharmadhikari G, Grün D, et al. A single-cell transcriptome atlas of the human pancreas. Cell Syst 2016;3:385–394.e3

27. Segerstolpe Å, Palasantza A, Eliasson P, et al. Single-cell transcriptome profiling of human pancreatic islets in health and type 2 diabetes. Cell Metab 2016;24:593–607
28. Persaud SJ, Liu B, Sampaio HB, Jones PM, Muller DS. Calcium/calmodulin-dependent kinase IV controls glucose-induced Irs2 expression in mouse beta cells via activation of cAMP response element-binding protein. Diabetologia 2011;54:1109–1120
29. Blanchet E, Van de Velde S, Matsumura S, et al. Feedback inhibition of CREB signaling promotes beta cell dysfunction in insulin resistance. Cell Rep 2015;10:1149–1157
30. Almers W. Gating currents and charge movements in excitable membranes. Rev Physiol Biochem Pharmacol 1978;82:96–190
31. Cole KS. *Membrane, Ions and Impulses: A Chapter of Classical Biophysics*. Berkeley, CA, University of California Press, 1968
32. Gautam D, Han SJ, Hamdan FF, et al. A critical role for beta cell M3 muscarinic acetylcholine receptors in regulating insulin release and blood glucose homeostasis in vivo. Cell Metab 2006;3:449–461
33. Namkung Y, Skrypnyk N, Jeong MJ, et al. Requirement for the L-type Ca(2+) channel alpha(1D) subunit in postnatal pancreatic beta cell generation. J Clin Invest 2001;108:1015–1022
34. Platzer J, Engel J, Schrott-Fischer A, et al. Congenital deafness and sinoatrial node dysfunction in mice lacking class D L-type Ca^{2+} channels. Cell 2000;102:89–97
35. Jeon D, Song I, Guido W, et al. Ablation of Ca^{2+} channel beta3 subunit leads to enhanced N-methyl-D-aspartate receptor-dependent long term potentiation and improved long term memory. J Biol Chem 2008;283:12093–12101
36. Shiao MS, Liao BY, Long M, Yu HT. Adaptive evolution of the insulin two-gene system in mouse. Genetics 2008;178:1683–1691
37. Sun P, Enslen H, Myung PS, Maurer RA. Differential activation of CREB by Ca^{2+}/calmodulin-dependent protein kinases type II and type IV involves phosphorylation of a site that negatively regulates activity. Genes Dev 1994;8:2527–2539
38. Yu X, Murao K, Sayo Y, et al. The role of calcium/calmodulin-dependent protein kinase cascade in glucose upregulation of insulin gene expression. Diabetes 2004;53:1475–1481
39. Hang Y, Stein R. MafA and MafB activity in pancreatic β cells. Trends Endocrinol Metab 2011;22:364–373
40. Xu G, Chen J, Jing G, Shalev A. Thioredoxin-interacting protein regulates insulin transcription through microRNA-204. Nat Med 2013;19:1141–1146
41. Chen J, Saxena G, Mungrue IN, Lusis AJ, Shalev A. Thioredoxin-interacting protein: a critical link between glucose toxicity and beta-cell apoptosis. Diabetes 2008;57:938–944
42. Zong H, Wang CC, Vaitheesvaran B, Kurland IJ, Hong W, Pessin JE. Enhanced energy expenditure, glucose utilization, and insulin sensitivity in VAMP8 null mice. Diabetes 2011;60:30–38
43. Zhu D, Xie L, Kang Y, et al. Syntaxin 2 acts as inhibitory SNARE for insulin granule exocytosis. Diabetes 2017;66:948–959
44. Zhu D, Zhang Y, Lam PP, et al. Dual role of VAMP8 in regulating insulin exocytosis and islet β cell growth. Cell Metab 2012;16:238–249
45. Schmidt HH, Warner TD, Ishii K, Sheng H, Murad F. Insulin secretion from pancreatic B cells caused by L-arginine-derived nitrogen oxides. Science 1992;255:721–723
46. Nead KT, Li A, Wehner MR, et al.; BioBank Japan, AGEN-BMI, GIANT Consortium. Contribution of common non-synonymous variants in PCSK1 to body mass index variation and risk of obesity: a systematic review and meta-analysis with evidence from up to 331 175 individuals. Hum Mol Genet 2015;24:3582–3594
47. Street VA, Bosma MM, Demas VP, et al. The type 1 inositol 1,4,5-trisphosphate receptor gene is altered in the opisthotonos mouse. J Neurosci 1997;17:635–645
48. Ye R, Ni M, Wang M, et al. Inositol 1,4,5-trisphosphate receptor 1 mutation perturbs glucose homeostasis and enhances susceptibility to diet-induced diabetes. J Endocrinol 2011;210:209–217
49. Reddy MV, Wang H, Liu S, et al. Association between type 1 diabetes and GWAS SNPs in the southeast US Caucasian population. Genes Immun 2011;12:208–212
50. Roach JC, Deutsch K, Li S, et al.; Swedish Childhood Diabetes Study Group; Diabetes Incidence in Sweden Study Group. Genetic mapping at 3-kilobase resolution reveals inositol 1,4,5-triphosphate receptor 3 as a risk factor for type 1 diabetes in Sweden. Am J Hum Genet 2006;79:614–627